



LAWRENCE
LIVERMORE
NATIONAL
LABORATORY

Molybdenum Sound Velocity and Shear Strength Softening under Shock Compression

J. H. Nguyen, M. C. Akin, R. Chau, D. E. Fratanduono, W. P. Ambrose, O. V. Fat'yanov, P. D. Asimow, N. C. Holmes

November 21, 2013

Physical Review B

Disclaimer

This document was prepared as an account of work sponsored by an agency of the United States government. Neither the United States government nor Lawrence Livermore National Security, LLC, nor any of their employees makes any warranty, expressed or implied, or assumes any legal liability or responsibility for the accuracy, completeness, or usefulness of any information, apparatus, product, or process disclosed, or represents that its use would not infringe privately owned rights. Reference herein to any specific commercial product, process, or service by trade name, trademark, manufacturer, or otherwise does not necessarily constitute or imply its endorsement, recommendation, or favoring by the United States government or Lawrence Livermore National Security, LLC. The views and opinions of authors expressed herein do not necessarily state or reflect those of the United States government or Lawrence Livermore National Security, LLC, and shall not be used for advertising or product endorsement purposes.

Molybdenum Sound Velocity and Shear Modulus Softening under Shock Compression

Jeffrey H. Nguyen¹, Minta C. Akin¹, Ricky Chau¹, Dayne E. Fratanduono¹,
W. Patrick Ambrose¹, Oleg V. Fat'yanov², Paul D. Asimow², Neil C. Holmes¹

1) Lawrence Livermore National Laboratory, Livermore, California, USA and

2) California Institute of Technology, Pasadena, California, USA

(Dated: May 1, 2014)

We measured the longitudinal sound velocity in Mo shock compressed up to 4.4 Mbar on the Hugoniot. Its sound speed increases linearly with pressure up to 2.6 Mbar; the slope then decreases up to the melting pressure of ~ 3.8 Mbar. This suggests a decrease of shear modulus before the melt. A linear extrapolation of our data to 1 bar agrees with the ambient sound speed. The results suggest that Mo remains in the *bcc* phase on the Hugoniot up to the melting pressure. There is no statistically significant evidence for a previously reported *bcc* \rightarrow *hcp* phase transition on the Hugoniot.

PACS numbers: 64.30.Ef, 62.50.Ef

I. INTRODUCTION

Interest in complete equations of state and phase diagrams for transition metals such as Ta, Fe, Cu, and Mo has recently surged. These metals have high melting temperatures at elevated pressures (P) and are stable to high P in diamond anvil cell (DAC) experiments, making them model candidates for studies at extreme conditions. To this end, many experiments and calculations have been published that address the high P melt curves and existence of high P phases^{1–23}.

These findings are controversial and often contradictory. The reports of "flat" melt curves for these metals^{1,2} are several thousand degrees below those previously reported^{3–6,8,9} and disagree with melting predicted by the Lindemann criterion²⁴. DAC studies show that Mo remains *bcc* up to 5.6 Mbar at room temperature⁹. Hixson *et al.*³ reported a *bcc* \rightarrow *hcp* crystal structure transition at 2.1 Mbar (≈ 4100 °K) and *hcp* \rightarrow liquid at 3.9 Mbar ($\approx 10,000$ °K) in their measurements of longitudinal sound speed (C_L) in shock-compressed Mo. However, similar work in Fe showed that such a solid \rightarrow solid transition depended on sample purity^{7,8}. No such solid \rightarrow solid transition is observed in Ta⁶ or Cu²⁵ sound speed data. Theoretical studies disagree on the relative stability of the *bcc* and *fcc* phases^{17,21} or require the experimentally observed solid \rightarrow liquid transition^{3,4} to be ignored or reinterpreted¹⁵.

High P DAC crystallographic experiments on Mo are restricted to room temperature⁹, or to ~ 1 Mbar at high temperature (T)^{1,2}, so the Hixson *et al.*³ study anchors the high P, T work. However, extrapolation of their results to ambient conditions disagrees with the measured ambient C_L by ~ 2 km/s. If correct, this would suggest a phase transition at $P < 1$ Mbar, which has neither been predicted or observed. This discrepancy between observed and extrapolated sound speed values may have arisen from the use of asymmetric impactors, which increases the uncertainty in C_L by incorporating the uncertainties in the impactor Hugoniot and sound velocities. While the recent work by Kleiser *et al.*¹⁰ appears to con-

firm Hixson *et al.*'s³ results, the experimental design is such that it would be unable to detect faster C_L that would contradict those results. It is therefore prudent to repeat the experiment using the latest technology and symmetric impactors to confirm or reject the existence of the reported phase transitions.

II. METHODS

The longitudinal sound velocity C_L is related to material properties by:

$$C_L = \left(\frac{K}{\rho} + \frac{4}{3} \frac{G}{\rho} \right)^{1/2} \quad (1)$$

where K and G are the bulk and shear moduli, respectively, and ρ is the material density. C_L is sensitive to changes in crystal structure since either or both K and G change with phase. Indeed, C_L measurements are used to determine melting on the Hugoniot since $G \approx 0$ in the fluid^{3,6–8}.

The experiment is based on the idea that the velocity of a rarefaction wave is faster than the initial shock wave in the laboratory frame²⁶. Since $U_s < C_L + U_p$, the rarefaction wave eventually overtakes the shock front. Both mass velocity, U_p , and shock velocity, U_s , are known from previous experiments⁴.

We need to determine the sample thickness D required for a rarefaction wave moving at $C_L + U_p$ to overtake the shock front (Figure 1) in Mo. Since we cannot directly observe the rarefaction wave catching up to the shock wave inside the metal, we observe this catch-up in bromoform (CHBr₃), the analyzer fluid, in contact with the sample. In Fig. 1, CHBr₃ fills the region between the sample and window. When the shock enters the CHBr₃, the CHBr₃ emits light at an intensity proportional to $U_{p,Br}^{7,8}$ where $U_{p,Br}$ is the CHBr₃ mass velocity²⁷. This provides a sharp increase in emission upon shock breakout and abruptly decreases when the release catches up to the shock front and weakens it. The time interval between the onset of emission and the abrupt decrease, Δt ,

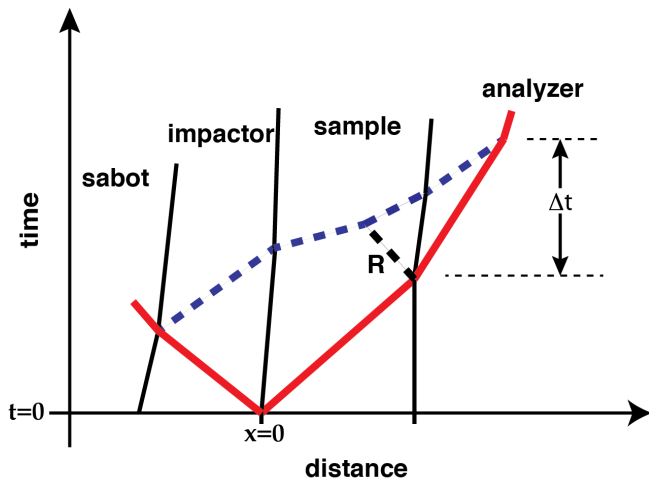


FIG. 1: $x-t$ diagram showing a rarefaction wave moving at $C_L + U_p$ (dashed blue line) overtaking the shock wave moving at U_s (solid red line) in the sample and analyzer in the laboratory rest frame. Bold black lines show the position of the interfaces between the impactor and sample target layers. Projectile impact on the target occurs at $(x, t) = (0, 0)$. The time interval between the arrival of the shock at the sample-analyzer interface and the overtake of the shock by the rarefaction wave is Δt . The rarefaction wave labeled R arises from the shock impedance mismatch between the sample and analyzer.

depends upon the thickness of Mo transited. This idea was used in previous sound speed experiments^{3,6–8,26}. Because the analyzer has a lower shock impedance (ρU_s) than the Mo sample, a backwards-going rarefaction wave is formed when the shock arrives at the sample/analyzer interface, labelled as “R” in Fig. 1. That rarefaction wave perturbs the velocity of the overtaking wave used to determine sound velocity. The experiment is designed so that we can determine the value of D for which the catch-up rarefaction and the shock arrive at the sample/analyzer interface simultaneously ($\Delta t = 0$) for each experiment, and minimize its uncertainty.

From D , we can determine the sound speed at the shock pressure,

$$C_L = \frac{\rho_0}{\rho} \frac{D + d}{D - d} U_s \quad (2)$$

where ρ_0 and ρ are initial and shocked densities, d is the impactor thickness, and U_s is shock speed in Mo.

The main source of uncertainty in C_L is the experimental determination of D . The value of Δt decreases linearly as the Mo sample thickness approaches D . We use a sample with varying Mo thickness, and find D by extrapolation of the measured catch-up times to $\Delta t = 0$. To improve accuracy, we use six thickness (Fig. 3) and use sample plates nearly as thick as D to minimize the extrapolation distance. Using six target steps requires extensive two-dimensional hydrodynamic simulations. These were carried out at various impactor velocities to ensure one-

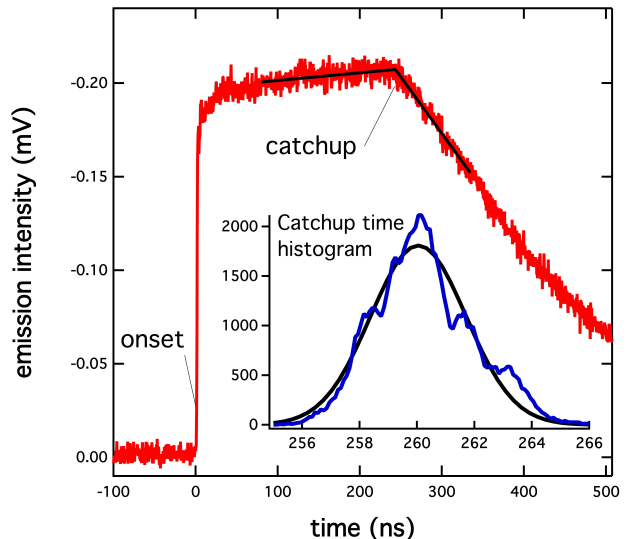


FIG. 2: Typical CHBr_3 emission. Intensity of emitted light is measured as a negative value. At the arrival of the shock front at the Mo- CHBr_3 interface, a rapid change in mass velocity, U_p , produces a correspondingly rapid rise in the intensity of light in the CHBr_3 analyzer (“onset”). Once the sound wave catches up to the shock wave (“catch-up”), the signal decreases. INSET: The calculated catch-up times from the randomly sampled fits are plotted as a histogram (blue). The Gaussian fit to the histogram (black) is used to determine Δt and σ for each channel. Δt and σ are then used to extrapolate to D as shown in Fig. 4.



FIG. 3: The Mo baseplate has 6 pockets of varying depth. Positions of the pockets are optimized to remove side release effects in the data. Each pocket is imaged at two spots near the pocket center, with each spot roughly $200 \mu\text{m}$ in diameter. The impactor approaches from the flat underside of the target, obscured in this view. The pocket diameters vary from 6 mm to 10 mm. Baseplate diameter is 32 mm.

dimensional hydrodynamic flow in the observation area prior to the catch-up event.

A two-stage light-gas gun launched 0.8-mm thick impactors at the target²⁸. At impact, two shock waves are generated, one into the stepped sample, the other into the impactor (solid red lines in Fig. 1). The shock moves through each target step into the CHBr_3 , which emits light. Meanwhile, the reverse-launched shock into the im-

pactor traverses the impactor thickness, where it arrives at the Mo/Lexan interface of the impactor, and launches a release wave. The head of the release wave (dashed blue line in Fig. 1) travels toward the CHBr_3 through the compressed Mo impactor and target at the local Mo sound speed, C_L .

The target and impactors were 99.99% pure Mo purchased from ESPI Metals. To achieve the highest pressure (4.4 Mbar), a Ta impactor was used instead of Mo. Targets comprise six countersunk pockets of varying thicknesses between 1.0 mm and 3.0 mm, depicted in Fig. 3. The baseplate was assembled in a liquid-tight container. We filled the detector side of the baseplate with degassed CHBr_3 . A fiber optic and lens assembly collected light at two distinct $\sim 200 \mu\text{m}$ diameter spots behind each pocket, for a total of twelve measurements.

Onset is easily identified. To find the catch-up time (Fig. 2), the intersection of two linear segments is calculated as described in Akin and Nguyen²⁹. The primary source of uncertainty in Δt and C_L arises from this calculation. To determine this calculation's impact, we use a Monte Carlo sampling algorithm. The results are tabulated and fit to a Gaussian distribution (inset, Fig. 2). The mean and standard deviation of that Gaussian function are used as the catch-up time and uncertainty (σ) in finding Δt . Extrapolation of a σ -weighted linear fit to Δt 's dependence on step height determines the catch-up distance D (Fig. 4). In cases where non-Gaussian character (e.g., a boxy or bimodal distribution) was seen, we chose a broader σ Gaussian fit to overestimate the σ used in extrapolation while capturing the mean sampled catch-up time.

Equation 2 uses D to find C_L at the experimental pressure. Previous studies of the Mo Hugoniot⁴ provided a straightforward way to determine P , ρ and their uncertainties given only impactor velocities. Uncertainties in D , ρ , and the Mo Hugoniot are propagated to find the uncertainty of C_L , σ_{C_L} , typically 0.5% in this study.

III. RESULTS AND DISCUSSION

We plot the new C_L data with those of Hixson *et al.*³ in Figure 5. New data are also listed in Table I. The Hixson data are further differentiated by impactor type for each shot. Over the range of $1.8 < P < 3.5$ Mbar, the data agree within their respective uncertainties. The reader may observe the increased error bars above 300 GPa on shots 450, 451, 4166, and 4168. The increased error on shots 450 and 4166 are due to attenuated light signals. On shot 450 this was due to a poorer quality (i.e., darker) batch of bromoform, which attenuates light signals. Data signals on shot 4166 were attenuated due to switching filters with a location change (Caltech to LLNL). Data signals on shot 4168 were not attenuated, but 4168 used a Ta impactor, which leads to a comparable increase in uncertainty. Shot 451's larger uncertainty is due to differences between channel-to-channel times

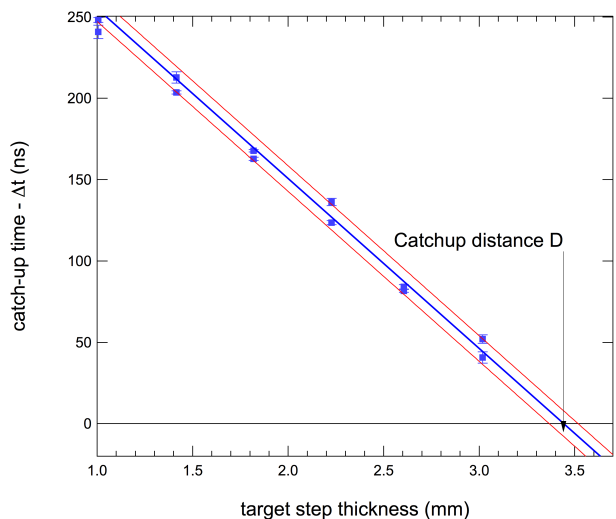


FIG. 4: Catch-up time Δt as a function of Mo baseplate step thickness. Extrapolated to $\Delta t = 0$, it yields the sample thickness at which catch-up takes place at the Mo sample/analyzer boundary, D .

on the two thicker steps. Masking these steps leads to calculated sound speeds of 9.65-9.85 km/s.

We note three significant differences between these new C_L data and Hixson *et al.*'s³. First, model statistics do not support a solid→solid phase transition at 2.1 Mbar. Second, the C_L vs. ρ slope, for $P < 2.6$ Mbar is significantly lower than that of Hixson *et al.*³; this pressure range includes the putative solid→solid transition. Third, C_L ceases increasing linearly above ~ 2.6 Mbar. We will examine each of these points in detail.

To address the existence of a solid→solid phase transition at 2.1 Mbar³, we proposed eight statistical models supporting a phase transition (two solid phases) and one model debunking this same phase transition (one solid phase). The models and associated statistical analyses are included in the appendix below. The latter model follows Birch's law, a linear approximation to the sound speed equation^{30,31}. This model agrees well with our data. The two-phase models also capture all the data. However, as argued in the appendix, it is more likely that the two-phase models fit the noise in the data rather than the underlying physics. We therefore cannot reject a simpler model of no phase transition in favor of a two-phase system.

The discrepancy between our results and those of Hixson *et al.*³ can be partly explained by their use of asymmetric impactors. In a symmetric impact experiment, Mo impactor on Mo sample, C_L can be determined from Eq. 2 where only the Mo Hugoniot shock speed, U_S , and density, ρ , are unmeasured. In non-symmetric experiments, two additional variables from the impactor, C_L^i and U_S^i , must be used to find C_L , increasing uncertainties significantly. In Hixson *et al.*'s³ data, the key point

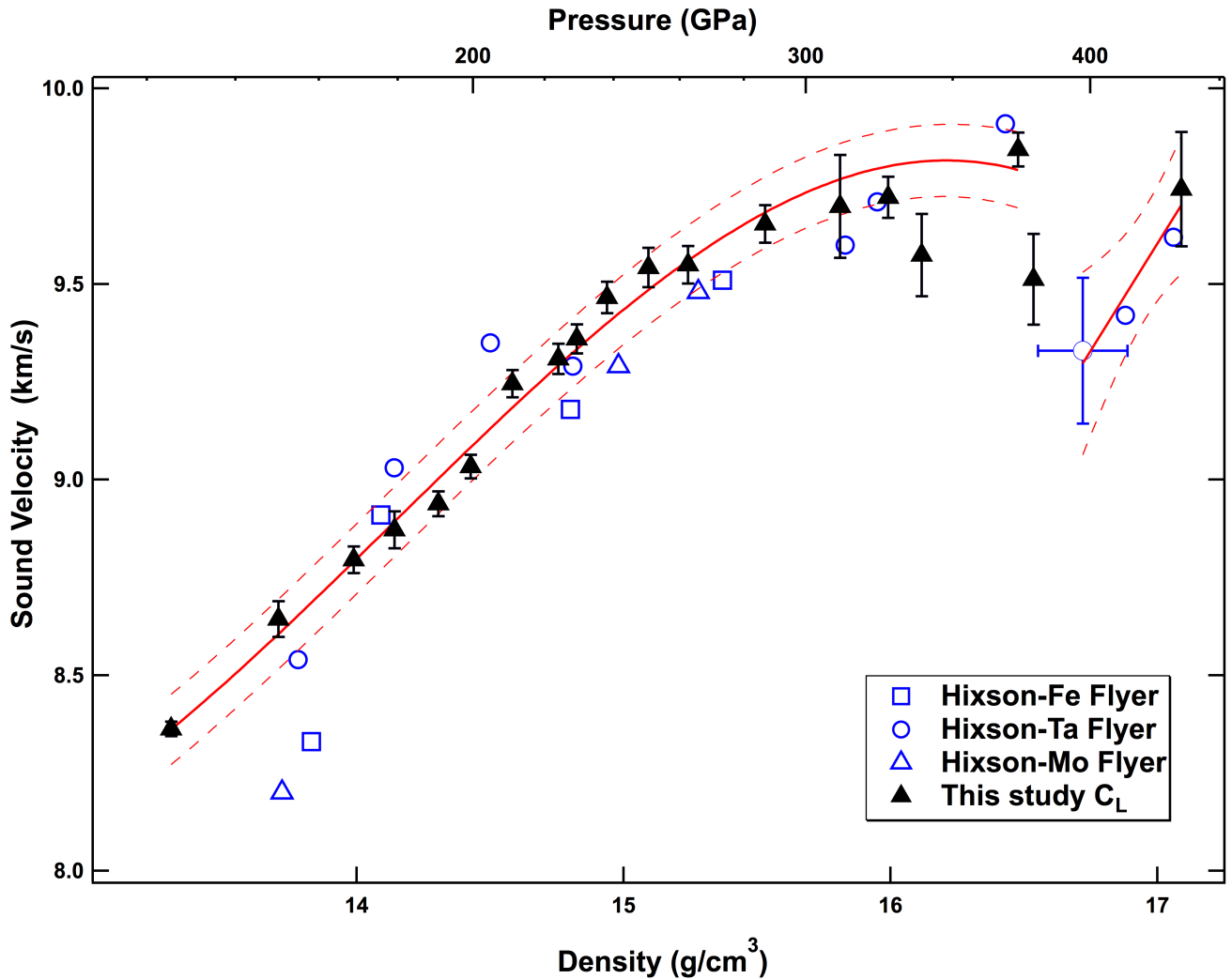


FIG. 5: Mo Sound Speed as a function of P and ρ . Solid symbols represent our data; open symbols are Hixson *et al.*'s data. The latter data are further differentiated by impactor used. Hixson's data error bars are nominally 2%³, and are shown on only one data point for clarity. 1- σ prediction bands are included in a fit to our data below the melting pressure. A linear fit with Hixson's data³ is also shown above the melting pressure. A single data point at 16.54 g/cc was not used in either fit.

at the putative solid-solid phase transition (2.1 Mbar, or 14.6 g/cc) is from a non-symmetric impact experiment.

Flat melt curve interpretations^{1,2,15} depend on the existence of a phase transition at 2.1 Mbar, and are inconsistent with the melt transition at 3.9 Mbar³. Extrapolation of Hixson's C_L to ambient Mo ρ_0 results in a value much lower than the ambient C_L of 6.25 km/s, due to the high b . This implies another solid \rightarrow solid transition, and that the existing phase on the Hugoniot is not *bcc* at P immediately below 2.1 Mbar. Alternately, pressure-induced $s \rightarrow d$ electronic transfer was considered the cause of this anomalous behavior^{3,32}. Linear extrapolation of the new data (with the lower b) to ambient yields $C_L = 6.3 \pm 0.15$ km/s. This is consistent with the hypothesis that Mo remains in the *bcc* phase at $P \lesssim 2.6$ Mbar, and does not support a flat melt curve interpretation. This result is supported by preliminary x-ray diffraction

work showing Mo is *bcc* at ~ 3 Mbar³³.

Above ~ 2.9 Mbar, these data suggest a decreasing shear modulus in Mo, shown by a decrease in b from 2.9 Mbar to the melt curve. This behavior was seen in Cu sound speed experiments²⁵, and is consistent with a predicted decrease of shear modulus prior to melt. Shear-wave velocity in the Earth's inner core also decreases near the melting pressure-temperature. Martorell *et al.*³⁴ attributed this decrease in elastic properties of hcp-Fe. For Mo in particular, our sound speed results are consistent with calculations by Cazorla *et al.*¹⁷ showing that the *bcc* phase is more stable than the *fcc* phase up to 3.5 Mbar.

Shot No.	flyer velocity (km/s)	flyer thickness (mm)	shock velocity (km/s)	density (g/cc)	Pressure (GPa)	catch-up distance (mm)	Sound velocity (km/s)
465	3.3960(5)	0.8102(4)	7.273(10)	13.3040(14)	126.1(2)	4.053(13)	8.363(18)
464	3.876(1)	0.8108(4)	7.575(11)	13.7070(16)	149.8(2)	3.85(4)	8.64(5)
438	4.226(1)	0.804(1)	7.791(12)	13.9880(16)	168.1(3)	3.74(3)	8.80(3)
437	4.405(6)	0.802(1)	7.909(13)	14.141(5)	177.7(4)	3.69(4)	8.87(5)
422	4.614(6)	0.793(1)	8.031(14)	14.306(5)	189.2(5)	3.620(18)	8.94(3)
424	4.766(1)	0.789(1)	8.134(14)	14.4270(16)	197.7(4)	3.553(17)	9.03(3)
423	4.964(4)	0.785(1)	8.258(14)	14.583(4)	209.1(4)	3.399(19)	9.25(4)
426	5.184(1)	0.793(1)	8.396(15)	14.7550(17)	222.0(4)	3.42(2)	9.31(4)
425	5.273(3)	0.779(1)	8.452(15)	14.824(3)	227.3(5)	3.33(2)	9.36(4)
421	5.420(5)	0.788(1)	8.544(16)	14.938(4)	236.2(5)	3.32(2)	9.47(4)
443	5.622(13)	0.786(1)	8.671(18)	15.093(10)	248.6(9)	3.29(2)	9.54(5)
441	5.817(10)	0.802(1)	8.793(18)	15.241(8)	260.8(8)	3.38(2)	9.55(5)
477	6.201(5)	0.8000(1)	9.034(18)	15.530(4)	285.6(7)	3.35(3)	9.65(5)
450	6.582(1)	0.806(1)	9.273(19)	15.8110(17)	311.2(7)	3.40(9)	9.70(13)
480	6.829(5)	0.8106(5)	9.43(2)	15.991(4)	328.2(8)	3.44(3)	9.72(5)
451	7.002(3)	0.806(1)	9.54(3)	16.12(2)	340(2)	3.56(6)	9.57(10)
4167	7.513(2)	0.8080(4)	9.86(2)	16.478(3)	377.5(9)	3.442(18)	9.84(4)
4166	7.594(2)	0.8112(4)	9.91(2)	16.535(3)	383.5(9)	3.73(9)	9.51(12)
4168	7.625(2)	0.786(1)*	10.36(2)	17.089(3)	438(8)	4.66(2)	9.74(15)

TABLE I: Experimental data as presented in figure 5. *Shot 4168 was the only non-symmetric shot in this study. Shot 4168 used a 0.8 mm Ta impactor to shock Mo well into the liquid phase. Error bars on Shot 4168 are accordingly larger due to the additional uncertainties in the Ta Hugoniot. Shots 4166-4168 were done at LLNL, the rest were carried out at Caltech.

IV. CONCLUSIONS

We measured the longitudinal sound speed C_L of Mo shocked to 1.3 to 4.0 Mbar using symmetric impacts. A single non-symmetric impactor was used to shock Mo to 4.4 Mbar. The rate of change of sound speed with density is lower than that observed by Hixson *et al.*³ and extrapolates to the measured ambient C_L . It is consistent with a stable *bcc* phase to at least 3.4 Mbar. We see no evidence for a previously reported solid-solid phase transition at 2.1 Mbar^{3,10}. Instead, these data show a stable phase up to 3.4 Mbar, with decrease of the shear modulus starting as early as 2.6 Mbar.

V. ACKNOWLEDGMENTS

We thank R. Hixson and M. Ross for their useful discussions, and Papo Gelle, Mike Long, Russ Oliver, Bob Nafzinger, Paul Benevento, Sam Weaver, and Cory McLean for their dedicated effort. Lawrence Livermore National Laboratory is operated by Lawrence Livermore National Security, LLC, for the U.S. Department of Energy, National Nuclear Security Administration under Contract DE-AC52-07NA27344.

VI. APPENDIX: STATISTICAL ANALYSIS

Since previous work by Hixson *et al.*³ suggested a solid-solid phase transition at 2.1 Mbar, we fitted our sound speed data from 1.26 Mbar to 2.60 Mbar to single-phase models and two-phase models. The single-phase model

follows Birch's law, a linear approximation to the sound speed equations derived from lattice dynamics^{30,31},

$$C_L = a + b\rho \quad (3)$$

where a and b are constants for a phase. Similarly, the two-phase model consists of two lines, one before and one after the phase transition,

$$C_L = \begin{pmatrix} a_1 + b_1\rho & \rho < \rho_{trans} \\ a_2 + b_2\rho & \rho > \rho_{trans} \end{pmatrix} \quad (4)$$

Strictly speaking, the one and two-phase models cannot be treated as nested due to their different functional forms, and so tests such as the likelihood ratio, F-test, or χ^2 -difference tests are invalid. However, we can compare the relative quality of fit for these models to the single phase model and make some estimates regarding the value of the more complicated model. We chose to do so through the χ^2 statistic,

$$\chi^2 = \Sigma \left(\frac{C_{L,obs} - C_{L,model}}{\sigma_{obs}} \right)^2. \quad (5)$$

We also calculated the probability $Q_{\chi^2, \nu}$ that a larger calculated χ^2 for the fit would be observed due to chance,

$$Q_{\chi^2, \nu} = [2^{\nu/2} \Gamma(\frac{\nu}{2})]^{-1} \int_{\chi^2}^{\infty} (t)^{\frac{\nu}{2}-1} e^{-\frac{t}{2}} dt. \quad (6)$$

where ν is the number of degrees of freedom (data points - independent variables) and $\Gamma(x) = \int_0^{\infty} (t)^{x-1} e^{-t} dt$. We tested this model for phase transition at different densities. The resulting χ^2 and $Q_{\chi^2, \nu}$ values, as well as the

calculated sound speed at ambient pressure, $C_{L,0}$, are tabulated in Table II for each fit. One of the single-phase models is included for comparison.

All of the models adequately capture the data. We then apply both statistic and physical tests to determine the correct model for this set of data. From a statistical point of view, the additional fit parameter of the two-phase models will lead to improved χ^2 values compared to the single phase model, as is shown in Table II. Such additional fit parameters increase the ability to fit noise in the data as well as the underlying physics. Because the single-phase model is sufficient to explain and predict the results, indicating that the physics has been adequately modeled, the additional complexity of a two-phase model is not justified. A specific case of Model 5 will be discussed below. From a physics point of view, the single-phase model agrees with Birch's law best on extrapolation to ambient sound velocity, $C_{L,0}$. We therefore select the single-phase model.

There is a large difference in the χ^2 value of the single-phase model and Model 5 (table II) which corresponds

to a phase transition near the putative transition at 2.1 Mbar. This model has an unusually small χ^2 statistic, which may encourage some readers to accept it as the "correct" model, and to argue that a transition exists at this pressure as a result. If we assume that Model 5 were a perfect model of the actual underlying physics of the transition, and we repeated the experiment with similar levels of precision, we would obtain a χ^2 value this size less than 3% of the time. It is more likely that Model 5 is fitting noise in the data, rather than underlying physics. Given the good agreement of the single phase fit, we cannot reject the simpler hypothesis of a single phase in favor of a two-phase system. Additional sound speed data in the 14.1-14.7 g/cc density range, of better than 0.1% accuracy and precision, would be needed to further resolve these models. These authors feel that even with the improved design and analysis techniques presented here, such data would need to be taken at impractically frequent spacings, that we prefer an alternate diagnostic method.

-
- ¹ D. Errandonea, B. Schwager, R. Ditz, C. Gessman, R. Boehler, and M. Ross, *Phys. Rev. B* **63**, 132104 (2001).
 - ² D. Santamaria-Perez, M. Ross, D. Errandonea, G. D. Mukherjee, M. Mezouar, and R. Boehler, *J. Chem. Phys.* **130**, 124509 (2009).
 - ³ R. S. Hixson, D. A. Boness, J. W. Shaner, and J. A. Moriarty, *Phys. Rev. Lett.* **62** (6), 637 (1989).
 - ⁴ R. S. Hixson and J. N. Fritz, *J. Appl. Phys.* **71** 1721 (1992).
 - ⁵ A. C. Mitchell and W. J. Nellis, *J. Appl. Phys.* **52**, 3363 (1981).
 - ⁶ J. M. Brown and J. W. Shaner, in *Shock Waves in Condensed Matter – 1983*, edited by J. R. Asay, R. A. Graham, and G. K. Straub (Elsevier, New York, 1984), p. 91.
 - ⁷ J. M. Brown and R. G. McQueen, *Geophys. Res. Lett.* **7** (7), 533 (1980).
 - ⁸ J. H. Nguyen and N. C. Holmes, *Nature* **427**, 339, (2004).
 - ⁹ Y. K. Vohra and A. L. Ruoff, *Phys. Rev. B* **42**, 8651 (1990).
 - ¹⁰ G. J. Kleiser, L. C. Chhabildas, W. D. Reinhart, and W. W. Anderson, *Shock Compression of Condensed Matter* **1426** 1517 (2012).
 - ¹¹ D. Errandonea, *Physica B* **357**, 356 (2005).
 - ¹² D. Errandonea, M. Somayazulu, D. Hausermann, and H. K. Mao, *J. Phys. Condens. Matter* **15**, 7635 (2003).
 - ¹³ S. P. Marsh, S.P., LASL Shock Hugoniot Data. University of California Press, Berkeley, pp. 658 (1980).
 - ¹⁴ R. G. McQueen, S. P. Marsh, J. W. Taylor, J. N. Fritz, W. J. Carter, In: Kinslow, R. (Ed.), *High Pressure Impact Phenomena*. Academic Press, New York, pp. 293. (1970).
 - ¹⁵ M. Ross, D. Errandonea, and R. Boehler, *Phys. Rev. B* **76** 184118 (2007).
 - ¹⁶ F. Jona and P. M. Marcus, *J. Phys. Cond. Matter* **17**, 1049 (2005).
 - ¹⁷ J. C. Cazorla, M. J. Gillan, S. Taioli, and D. Alfè, *Phys. Rev. B* **85**, 064113, (2012).
 - ¹⁸ J. C. Cazorla, M. J. Gillan, S. Taioli, and D. Alfè, *J. Chem. Phys.* **126**, 194502, (2007).
 - ¹⁹ C. J. Wu, P. Söderlind, J. N. Glosli and J. E. Klepeis, *Nat. Mater.* **8** 223, (2009).
 - ²⁰ S. Japel, B. Schwager, R. Boehler, and M. Ross, *Phys. Rev. Lett.* **95**, 167801 (2005).
 - ²¹ A. B. Belonoshko, S. I. Simak, A. E. Kochetov, B. Johansson, L. Burakovsky, and D. L. Preston, *Phys. Rev. Lett.* **92**, 195701 (2004).
 - ²² J. A. Moriarty, *Phys. Rev. B* **45** (5), 2004 (1992).
 - ²³ C. E. Ragan, M. G. Silbert, and B. C. Diven, *J. Appl. Phys.* **48** 2860 (1977).
 - ²⁴ F. Lindemann, *Z. Phys.*, **11**, 609, (1910).
 - ²⁵ D. Hayes, R. S. Hixson, and R. G. McQueen, in *Shock Compression of Condensed Matter – 1999*, edited by M. D. Furnish, L. C. Chhabildas, and R. S. Hixson (American Institute of Physics, Melville, New York, 2000), p. 483.
 - ²⁶ R. G. McQueen, J. W. Hopson, and J. N. Fritz, *Rev. Sci. Instrum.* **53** 245 (1982).
 - ²⁷ R. G. McQueen and D. G. Isaak, in *Shock Waves in Condensed Matter – 1983*, edited by S. C. Schmidt, J. N. Johnson and L. W. Davison, (Albuquerque, NM 1989) p.125. New York, 1984), p. 91.
 - ²⁸ A. H. Jones and W. M. Isbell, *J. Appl. Phys.* **37**, 3493 (1966).
 - ²⁹ M. C. Akin and J. H. Nguyen, *to be published* (2013).
 - ³⁰ D. L. Anderson, *Geophys. J. R. Astron. Soc.* **13** 9 (1967).
 - ³¹ T. J. Shankland and D. H. Chung, *Phys. Earth Planet. Int.* **8** 121 (1974).
 - ³² B. K. Godwal and R. Jeanloz, *Phys. Rev. B* **41** 7440 (1990).
 - ³³ J. Wang, F. Coppari, R. F. Smith, J.H. Eggert, T. Boehly, G. Collins, and T. S. Duffy, *AGU Fall Meeting abstract* (2014).
 - ³⁴ B. Martorell, L. Voadlo, J. Brodholt, and I. G. Wood, *Science* **342** 466 (2013).

model no. two-phase	ρ_{trans}	χ^2	ν	$Q_{\chi^2, \nu}$	$C_{L,0}$
1	13.85	8.60	9	0.475	6.22
2	14.06	6.26	9	0.714	6.40
3	14.22	5.76	9	0.763	6.44
4	14.37	6.38	9	0.702	6.55
5	14.51	2.78	9	0.972	6.55
6	14.67	10.14	9	0.340	6.43
7	14.79	10.84	9	0.287	6.40
8	14.88	11.21	9	0.262	6.22
single phase	n/a	13.18	10	0.214	6.38

TABLE II: Goodness-of-fit results from nine models of sound speed data up to 15.15 g/cc. Models 1-8 assume a two-phase model with the phase transition occurring at ρ_{trans} . χ^2 values, degrees of freedom (ν), the probability of obtaining a larger χ^2 ($Q_{\chi^2, d}$), and extrapolation of the model to calculated the sound speed at ambient condition ($C_{L,0}$) are shown on the right.